PERGAMON

International Journal of Heat and Mass Transfer 45 (2002) 113–123

International Journal of HEAT and MASS TRANSFER

www.elsevier.com/locate/ijhmt

Effect of bulk flow pulsations on film cooling with compound angle holes

Joon Sik Lee *, In Sung Jung

Turbo and Power Machinery Research Center, School of Mechanical and Aerospace Engineering, Seoul National University, Seoul 151-742, Republic of Korea

Received 3 December 1999; received in revised form 9 March 2001

Abstract

Experiments are conducted to investigate the effects of bulk flow pulsations on film cooling with compound angle holes. A row of five film cooling holes is considered with orientation angles of 0°, 30°, 60°, and 90° at a fixed inclination angle of 35°. Static pressure pulsations are produced by an array of six rotating shutter blades, which extend across the span of the exit of the wind tunnel test section. The pulsation frequency is fixed at 36 Hz, but changes in the time-averaged blowing ratios of 0.5, 1.0 and 2.0 produce three different coolant Strouhal numbers, 3.6, 1.8 and 0.9, respectively. Detailed film cooled boundary layer temperature distributions are measured by a cold wire and the adiabatic film cooling effectiveness by thermochromic liquid crystal (TLC). The boundary layer temperature surveys show that pulsations induce large disruptions to the boundary layer temperature distribution and the film coverage. As the orientation angle increases, the injectant concentration spreads further into the spanwise direction because of pulsations than the steady case. With pulsations the adiabatic film cooling effectiveness value decreases regardless of the orientation angle. The amount of reduction, however, depends on the orientation angle in such a way that the larger the orientation angle is, the smaller the reduction is.

1. Introduction

Film cooling applied to gas turbine blades is known to be affected by many parameters such as free-stream condition, blowing ratio, blade surface curvature, flow unsteadiness, hole arrangement and configuration, and so forth. Nowadays people are getting more interested in film injection with compound angle orientations because it is supposed to provide more uniform and improved film coverage compared to that with simple angle injection. Uniform film coverage can be obtained because the coolant with compound angle orientation has a spanwise velocity component that spreads the coolant over the region between adjacent film holes.

Flow unsteadiness is another important parameter, which is most recently recognized to have dramatic effects on film cooling. Film cooling flows are subject to bulk flow pulsations that result in important variations of the static pressure near turbine airfoil surfaces as blade rows move relative to each other. As a result, coolant flow rates pulsate at film hole exits, and injectant trajectory and coverage vary with time downstream of the film holes. Such changes to film cooling protection and flow structure draw important consequences regarding design of film cooling systems for turbine blade surfaces.

Film cooling with compound angle orientations under steady conditions was surveyed by Sathyamurthy and Patankar [1], Ligrani et al. [2,3], Sen et al. [4], Schmidt et al. [5], Honami et al. [6], Ligrani and Lee [7], Ekkad et al. [8], Ligrani and Ramsey [9], and Lee et al. [10]. The above studies investigated flow characteristics, film cooling effectiveness, and iso-energetic heat transfer coefficient ratio at different blowing ratios with various hole arrangements and compound angle configurations. In general, their results show that compound angle injection provides substantial improvement in film coverage compared to the simple angle configuration at the same hole spacing, normalized streamwise location, and blowing ratio.

* Corresponding author.

0017-9310/02/$ - see front matter
PII: S0017-9310(01)00133-8

Nomenclature

D	injection hole diameter
f	pulsation frequency
L	injection hole length
M	time-averaged blowing ratio ($= U_c/U_\infty$)
P	static pressure
Re_D	injectant Reynolds number ($= U_c D/\nu$)
Re_X	free-stream Reynolds number ($= U_\infty X/\nu$)
St_c	injectant Strouhal number ($= 2\pi fL/U_c$)
T	temperature
t	time
U	velocity
X	distance from the trip wire to film hole center
x, y, z	streamwise, normal and spanwise coordinates

Greek symbols

α	inclination angle
β	orientation angle
η	adiabatic film cooling effectiveness ($= (T_{aw} - T_\infty)/(T_c - T_\infty)$)
Θ	dimensionless temperature ($= (T - T_\infty)/(T_c - T_\infty)$)
ν	kinematic viscosity
τ	pulsation period
ψ	pressure parameter ($= (\Delta P_{max} - DP_{min})/\Delta\bar{P}$)

Subscripts/superscripts

aw	adiabatic wall
c	injectant
0	plenum
∞	free-stream
–	spanwise-averaged or time-averaged
=	space-averaged
$\sim$	phase-averaged

Dunn et al. [11] and Rao et al. [12] conducted experiments to measure the time-resolved surface pressure for the vane and blade of a transonic single-stage research turbine. They observed large static pressure variations on the blade suction surface. The period of the pressure variation is the time for the blade to pass one vane passage. The effects of potential flow interactions and passing shock waves in altering the protections nominally provided by film cooling are described by Abhari and Epstein [13], Abhari [14], Ligrani et al. [15–17], and Sohn and Lee [18]. In an investigation of rotor heat transfer in a short-duration blow-down turbine test facility, Abhari and Epstein [13] indicate that flow pulsations cause the time-averaged heat transfer rate to increase by 12% on the suction surface and to decrease by 5% on the pressure surface compared to values measured with no pulsations. According to recent experiments by Ligrani et al. [15,16], flow visualization results evidence two distinct injectant flow regimes: quasi-steady and non-quasi-steady. For a single L/D ratio employed in their study, magnitudes of the injectant Strouhal number less than 1–2 correspond to quasi-steady injectant behavior, and the magnitudes greater than 1–2 correspond to non-quasi-steady behavior, regardless of the magnitude of the blowing ratio.

However, all the previous compound angle studies are conducted under steady conditions, and bulk flow pulsation studies are confined to simple angle injection. It can easily be expected that compound angle injection with imposed bulk flow pulsations provides different film coverage because the instantaneous injectant trajectory is supposed to oscillate obliquely in the spanwise direction with an inclination angle to the surface. On the other hand, with simple angle injection, the injectant trajectory oscillates simply in the streamwise/normal plane.

The present study investigates the effect of bulk flow pulsations on compound angle injection. Time- and phase-averaged temperature distributions are obtained in spanwise/normal planes in the streamwise direction, and the adiabatic film cooling effectiveness distributions are presented.

2. Experimental apparatus and procedures

A schematic of the wind tunnel and the injectant supply system is shown in Fig. 1(a). The wind tunnel is an open-circuit and subsonic one, with a 6.25:1 contraction ratio nozzle and an exit cross-section of 0.4×0.28 m^2. The nozzle leads to the test section, which is a rectangular duct 3.0 m long. At a free-stream velocity of 10 m/s, flow at the test section inlet shows excellent spatial uniformity with spanwise velocity variations less than 0.3%, and a turbulence level less than 0.2%. A boundary layer trip wire of 1.8 mm diameter is located on the test plate just downstream of the nozzle exit. The air, used as the injectant, first flows through an orifice followed by two heat exchangers that control the injectant temperature. The air is then ducted to a plenum chamber and discharged through the injection holes.

Static pressure pulsations are produced in the test section using an array of rotating shutter blades located at the exit of the test section and driven by a system of gears and an electric motor. With the bulk flow pulsation of 36 Hz, the coolant Strouhal number,

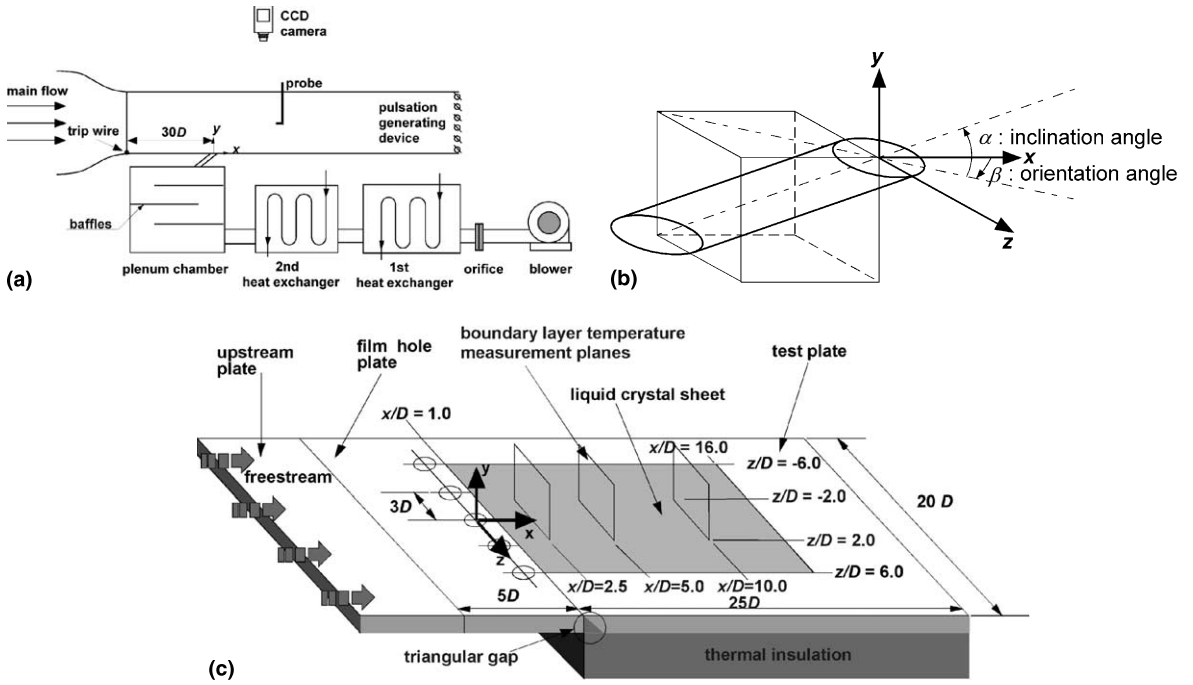

Fig. 1. Experimental set-up and film hole configuration.

$St_c = 2\pi fL/U_c$, varies from 0.9 to 3.6. Typical values for operating turbines range from 0.2 to 6.0. Coolant Strouhal numbers and non-dimensional pressure parameters according to the blowing ratios are listed in Table 1. Here the non-dimensional pressure parameter is defined as

$$\Psi = \frac{\Delta P_{\max} - \Delta P_{\min}}{\Delta \bar{P}}, \tag{1}$$

where ΔP is the instantaneous static pressure difference between the plenum and free-stream and $\Delta \bar{P}$ is the time-averaged value.

Experiments are conducted at a fixed free-stream mean velocity of 10 m/s. The injection hole diameter, D, is 20 mm and its length is $4D$. The Reynolds number, $Re_X = U_\infty X/v$, based on the distance between the trip wire and the hole center is 383 000. The boundary layer thickness (based on $0.99U_\infty$) at the hole center is $0.91D$, the displacement thickness is $0.14D$, and the momentum thickness is $0.10D$. The shape factor of the boundary layer is 1.4, which is the typical value of a fully developed turbulent boundary layer. The blowing ratio, M, is the ratio of the injectant mean velocity to free-stream mean velocity. The blowing ratio values considered in this study are 0.5, 1.0 and 2.0, and the corresponding injectant Reynolds numbers, $Re_D = U_c D/v$, are 6400, 12 700 and 25 400, respectively.

Table 1
Injectant Strouhal number (St_c) and pressure parameter (Ψ)

M	St_c	Ψ
0.5	3.60	8.83
1.0	1.80	3.43
2.0	0.90	1.03

The compound angle injection has two injection angles as shown in Fig. 1(b). The inclination angle, α, is defined as the angle between the injection vector and its projection on the x–z plane whereas the orientation angle, β, is defined as the angle between the streamwise direction and the projection of the injection vector on the x–z plane. The inclination angle is fixed at 35° and the direction of the orientation angle is in the $+z$-direction as described in Fig. 1(b). The film hole plates are prepared for each orientation angle of 0°, 30°, 60° and 90°. In each film hole plate, a row of five holes is located $30D$ downstream of the trip wire as shown in Figs. 1(a) and (c). The hole spacing between the hole centers is $3D$. As described in Fig. 1(c), the test plate consists of an upstream plate, one of four orientation angle film hole plates, and the measurement plate. The measurement plate starts at $x/D = 1.0$. To prevent the adiabatic wall temperature elevation near the downstream edge of the holes, the injection holes are machined in the film hole plate, not in the measurement plate. Polystyrene was formed in the triangular gap between the film hole plate and the measurement plate. The foamed polystyrene in the gap works as a thermal barrier that minimizes the

conduction from the injection holes to the measurement plate.

The adiabatic film cooling effectiveness is defined as follows:

$$\eta = \frac{T_{aw} - T_\infty}{T_c - T_\infty}, \tag{2}$$

where T_{aw} denotes the adiabatic wall temperature measured with liquid crystal.

A thermochromic liquid crystal (TLC) sheet is used to measure the temperature distribution on the entire surface downstream of the injection holes. The TLC sheet covers the test plate from $x/D = 1.0$ to $x/D = 16.0$, and from $z/D = -6.0$ to $z/D = 6.0$. The TLC sheet consists of 110-μm-thick polyester film, TLC coating, black paint, and adhesive layer. The total thickness of the sheet is 240 μm. A 12.7-mm-thick polycarbonate plate is attached just beneath the TLC sheet. Foamed polystyrene of 50 mm thickness is used for insulation. A CCD camera is used to capture TLC color images, which is aligned perpendicular to the TLC sheet 1.2 m away. Two 150 W halogen lamps are used to illuminate the TLC sheet.

Various techniques of TLC are available for temperature measurements. Among many techniques, the steady-state, hue capturing method is adopted in this study. The liquid crystal used to measure effectiveness distributions has a color-changing temperature range from 20°C to 30°C. Since the bandwidth of the TLC sheet is wide, the sheet can map the entire isothermal pattern of a surface from a single image. Robust TLC color–temperature response calibration, however, is necessary for high-accuracy measurements. It is known that the perceived color of a TLC depends on the lighting/viewing arrangement, the spectrum of the primary illuminant and background light, and the optical properties of the measurement path as well as temperature. When temperature was measured with the TLC, extra care was taken to fix all the conditions identical with the calibration to avoid the color variation problem.

The boundary layer temperature distribution is presented in terms of dimensionless temperature defined as

$$\Theta = \frac{T - T_\infty}{T_c - T_\infty}. \tag{3}$$

In the boundary layer temperature distribution measurements, the free-stream temperature is fixed at 20°C while the injectant is heated to 40°C. The density ratio of the injectant to free-stream resulting from the heating is 0.93. The boundary layer temperature distribution can show injectant behavior, and has a close relation with the effectiveness distribution on the wall. A 1 μm dia cold wire probe driven by a constant current anemometer is used to measure the temperature distributions. The calibrations of the cold wire system are performed using a platinum resistance thermometer. The measurement of boundary layer temperature distribution is taken at the three y–z planes at $x/D = 2.5, 5.0$ and 10.0, with $-2.0 \leqslant zD \leqslant 2.0$. In the y- and z-direction, the temperature data are distributed with a $0.2D$ spacing.

The uncertainty analysis is evaluated on 20 to 1 odds (95% confidence level). All the uncertainty values are evaluated from the method of single-sample experiments proposed by Kline and McClintock [19]. The uncertainty of the dimensionless boundary layer temperature is 6.4% at the typical Θ value of 0.25, and that of the adiabatic film cooling effectiveness is 6.8% at a typical η value of 0.2. The uncertainty value of the dimensionless boundary layer temperature is getting larger as the difference between the free-stream and the boundary layer temperatures becomes smaller. For example, the uncertainty value increases up to 28.8% at $\Theta = 0.05$. The same is true for the uncertainty value of the adiabatic film cooling effectiveness. The uncertainty value is 29.5% at $\eta = 0.05$.

3. Results and discussion

3.1. Bulk flow pulsation characteristics

The periodic characteristics of the phase-averaged free-stream static pressure are illustrated in Fig. 2. The data are presented for time-averaged blowing ratios of 0.5, 1.0 and 2.0 at a pulsation frequency of 36 Hz. Here, $\Delta\tilde{P}$ indicates the difference in the phase-averaged static pressure between the plenum and free-stream, $\tilde{P}_0 - \tilde{P}_\infty$, and $\Delta\bar{P}$ is the difference in time-averaged static pressures. The pressure data show quantitative alterations to waveforms, which occur as M is changed. The ratio of free-stream static pressure pulsations to time-averaged free-stream dynamic pressure is about 320% as shown in Fig. 2. Such variations evidence important coupling be-

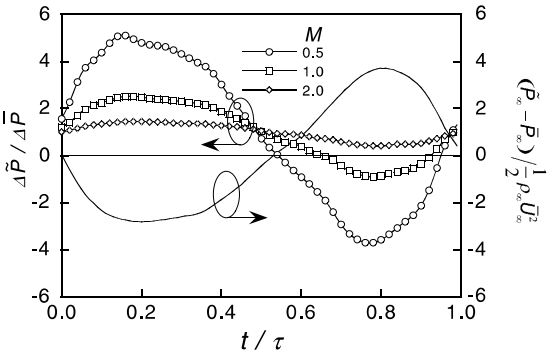

Fig. 2. Phase-averaged static pressure difference between plenum and free-stream.

tween the pulsations, and the film coolant in the holes and within the plenum. The amplitude of the pressure difference increases as the blowing ratio decreases.

Another important fact is that when the blowing ratios are 0.5 and 1.0, duration of negative values of $\Delta\tilde{P}$ is observed in a pulsation period. At $M = 0.5$, negative values are present over almost half a pulsation period. This implies that the free-stream static pressure could be higher than the plenum pressure, which might cause flow ingestion into the holes.

3.2. Boundary layer temperature distributions

Fig. 3 shows local film cooled boundary layer temperature distributions in a spanwise/normal plane at a downstream location of $x/D = 2.5$ at different instants in a pulsation period. The blowing ratio is 0.5 that corresponds to the coolant Strouhal number of 3.6. Note that the time in a pulsation period at which the highest temperature distribution (or highest injectant concentration) occurs is around $t/\tau = 0.8$ as shown in Fig. 3, while the maximum of the pressure difference takes place at $t/\tau = 0.2$ as in Fig. 2. The phase lag is caused due to two reasons. One is the fact that it takes time for the injectant to adjust itself to the pressure change because of the inertia of the injectant. The other is the fact that temperature distributions are measured at $x/D = 2.5$ not at the hole exit. Thus, the time during the injectant flows from the hole exit to $x/D = 2.5$ causes additional phase lag to the pressure variation.

The phase-averaged temperature distributions illustrate important changes to the instantaneous injectant mass flow rate subjected to free-stream static pressure pulsations. When the injectant issued with the lowest instantaneous blowing ratio reaches $x/D = 2.5$, the highest temperature regions are located very close to the wall. This is evidenced at $t/\tau = 0.4$ (Fig. 3(a)). In the portions of the pulsation in which the free-stream static pressure is lowest, the instantaneous blowing ratio is highest, and when the injectant issued with the highest instantaneous blowing ratio arrives at $x/D = 2.5$, the highest temperature regions are located slightly away

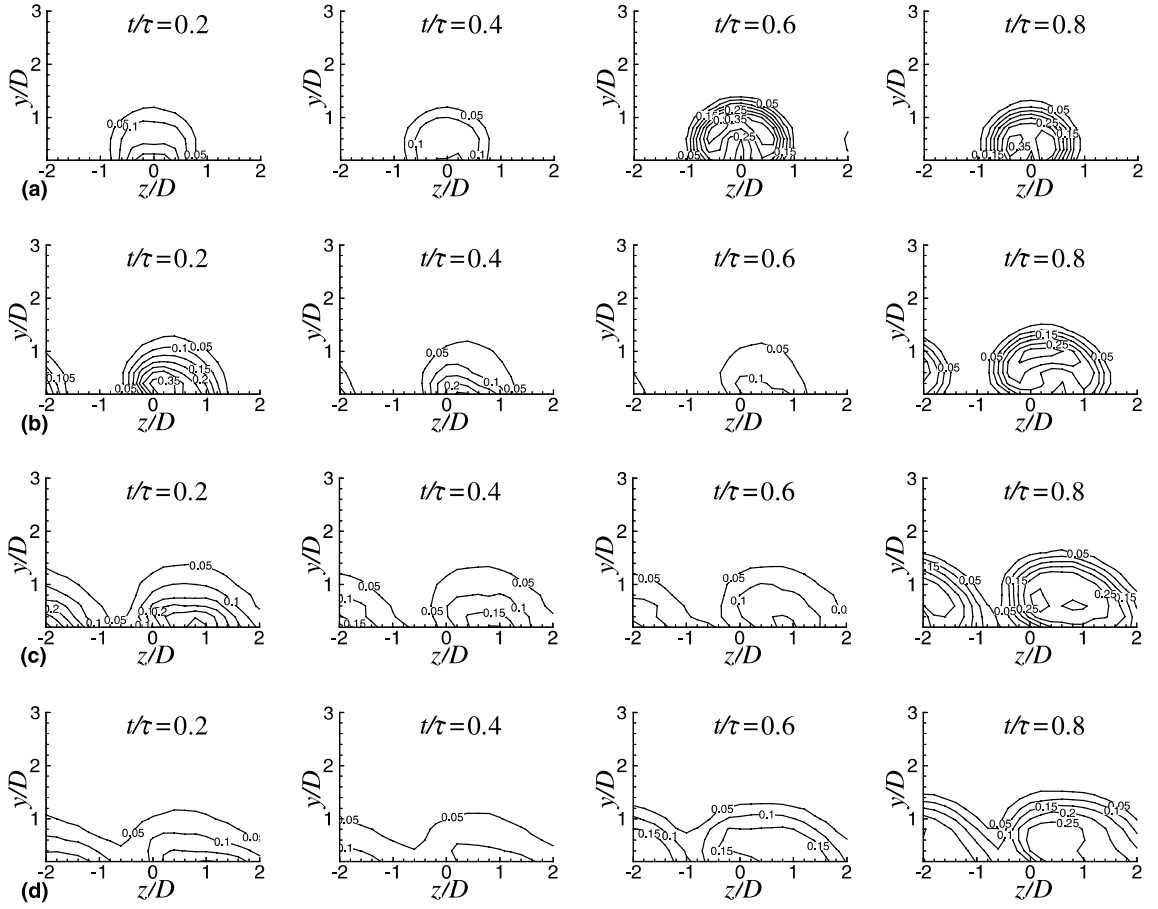

Fig. 3. Phase-averaged boundary layer temperature distributions at $x/D = 2.5$ for $M = 0.5$: (a) $\beta = 0°$; (b) $\beta = 30°$; (c) $\beta = 60°$; (d) $\beta = 90°$.

from the wall, as shown at $t/\tau = 0.6$ (Fig. 3(a)). These data thus illustrate how imposed bulk flow pulsations from potential flow interactions and passing shock waves cause the injectant to periodically lift-off from a turbine surface, which often causes the time-averaged film cooling effectiveness to decrease. This reduction in the film cooling effectiveness is due mainly to the massive oscillation of the injectant, which greatly increases mixing [15], over time.

As the orientation angle increases, the injectant concentration spreads further in the spanwise direction because of pulsations than the steady case. With compound angle injection, the injectant has a lateral (spanwise) component of momentum as well as a vertical component. When the mass flow rate is altered instantaneously during a pulsation period, the strength of the lateral momentum of the injectant is also altered. The injectant, thus, oscillates laterally with a periodic up-and-down motion. The lateral oscillation is not observed in simple angle injection, since simple angle injection does not produce lateral momentum. The lateral oscillation is expected to result in a more uniform effectiveness distribution though its magnitude decreases because of lateral diffusion of the injectant.

Fig. 4 compares time-averaged boundary layer temperature surveys with steady distributions (0 Hz). The data are obtained at $x/D = 2.5$ when $M = 0.5$. It is evidenced that 36-Hz pulsations produce remarkable disruptions to the temperature distributions and hence the film coverage. The injectant is attached fairly well to the wall and confined to $y/D \approx 1$ in the case of no pulsation. On the other hand, a considerable change is brought about when pulsations are imposed. For example, at $\beta = 60°$ (Fig. 4(c)), the isothermal contours rises to $y/D \approx 1.5$, and the maximum Θ value decreases to 0.15 from the steady value of 0.55. The diffusion of the injectant into the normal direction is caused partly by the time dependent up-and-down motion of injectant trajectory and partly by the enhanced turbulent mixing between the injectant and the free-stream fluid.

3.3. Adiabatic film cooling effectiveness distributions

Fig. 5 compares the adiabatic film cooling effectiveness distributions with and without pulsations at $M = 0.5$ for different compound angle injections. The effectiveness distributions downstream of injection holes alter remarkably at the high St_c of 3.6. The change can thus be observed when comparing the steady effectiveness distributions with the effectiveness distributions with 36-Hz pulsations. The steady film cooling effectiveness distributions show better film protection and high effectiveness values compared to unsteady one. As described by the boundary layer temperature distributions, the injectant is well attached to the wall at $M = 0.5$ since the normal momentum is relatively weak. The effectiveness distribution of simple angle injection shows symmetric distribution, however, as the orientation angle increases, the symmetry with respect to the hole center line is no longer maintained as shown in Figs. 5(b)–(d).

The effectiveness distributions in the steady case show that as the orientation angle increases from 0° to 30°, the lateral variation of the effectiveness decreases. The low effectiveness region between holes are large for simple angle injection, while the low effectiveness region is reduced as can be seen in the effectiveness distribution of the 30° compound angle injection. The effectiveness distribution of the lateral injection case ($\beta = 90°$) shows a fairly uniform distribution in the spanwise direction as shown in Fig. 5(d). Since the uniform effectiveness distribution is produced through the increment of effec-

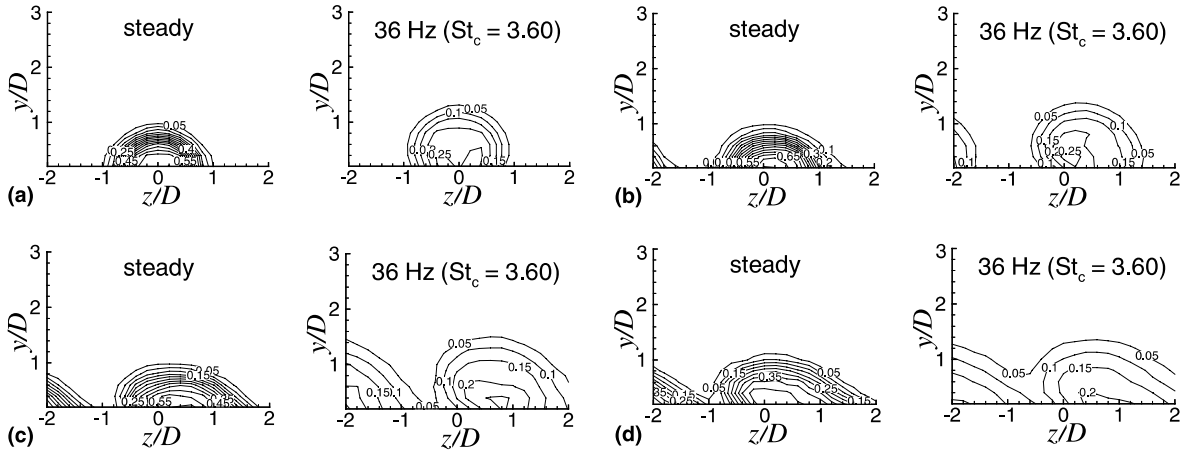

Fig. 4. Time-averaged boundary layer temperature distributions at $x/D = 2.5$ for $M = 0.5$: (a) $\beta = 0°$; (b) $\beta = 30°$; (c) $\beta = 60°$; (d) $\beta = 90°$.

tiveness in the low effectiveness region between holes as the orientation angle increases, the spanwise-averaged effectiveness should increase with the increasing orientation angle at $M = 0.5$.

With bulk flow pulsations, the effectiveness values are drastically reduced with the reduction in the case of simple angle injection being more significant. All unsteady effectiveness distributions become more uniform compared to steady distributions due to the additional spanwise spreading of the injectant with pulsations. The reduction in the effectiveness is mainly due to the decrease in the peak effectiveness. Comparison with the

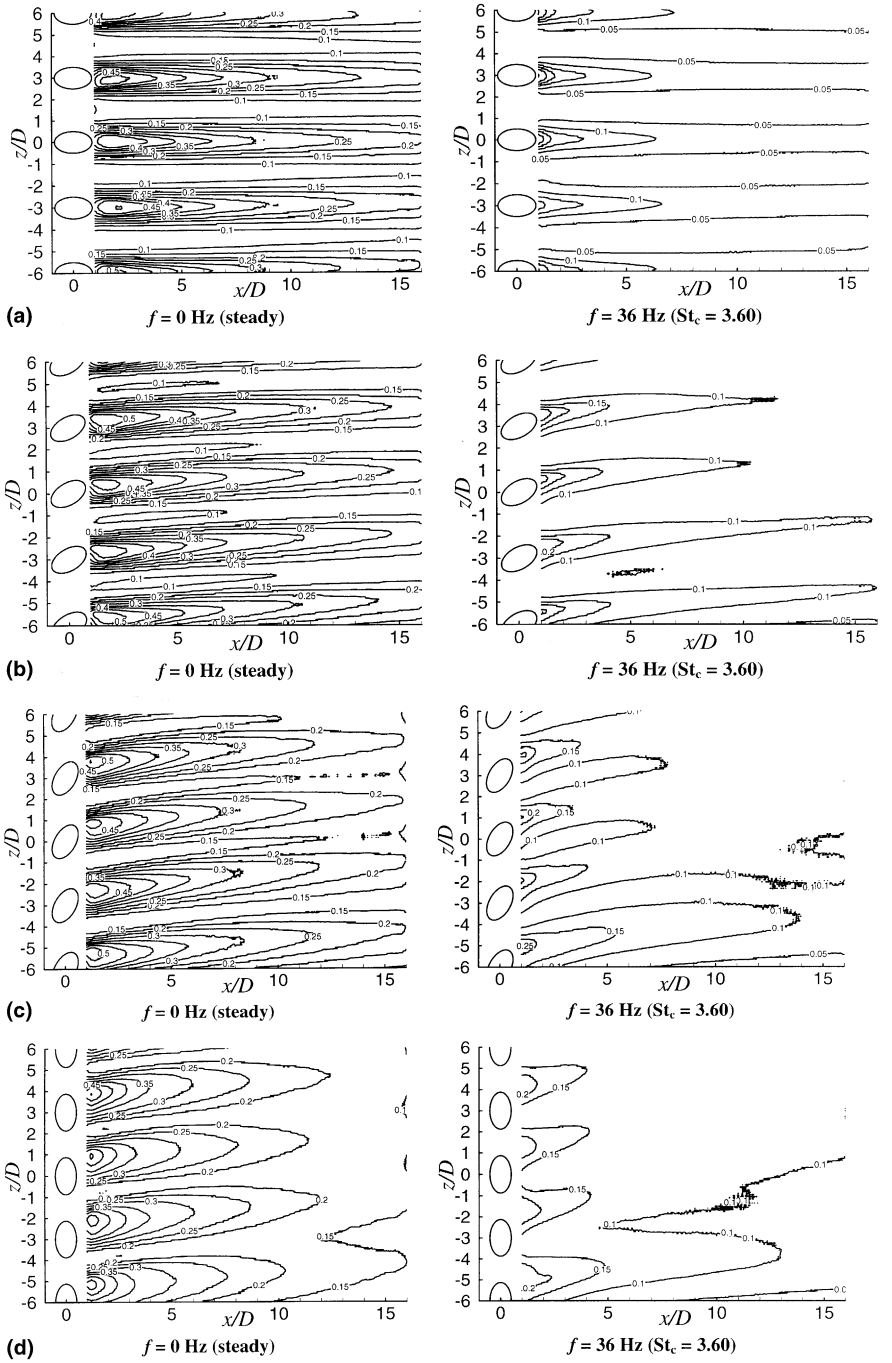

Fig. 5. Adiabatic film cooling effectiveness distributions for $M = 0.5$: (a) $\beta = 0°$; (b) $\beta = 30°$; (c) $\beta = 60°$; (d) $\beta = 90°$.

simple angle effectiveness distributions reveals that the low effectiveness region between holes is slightly reduced because of pulsations, but the high effectiveness value along the hole centerline is significantly reduced. This fact is common to all four compound angles. In the case of the 90° orientation angle injection, the low effectiveness values are nearly the same as shown in Fig. 5(d), but the peak effectiveness is also dramatically reduced. This is closely related to the boundary layer temperature distribution. As shown in Fig. 4, the peak temperature in the boundary layer is extremely dropped at the pulsation with $St_c = 3.6$. The enhanced mixing in the unsteady jet injected to cross-flow and the injectant oscillation in the y–z plane both lead to the decrease in the peak boundary layer temperature, and result in the low effectiveness at the high St_c. The reduction in the peak effectiveness due to the pulsations also induces smoothing effects on the effectiveness distribution.

Fig. 6 shows the local effectiveness distributions at $x/D = 5.0$ for $M = 0.5, 1.0$ and 2.0. Steady values are indicated by open symbols and unsteady ones by solid symbols. In general, the effectiveness distributions do not show any substantial changes from the steady distributions at St_c values below unity; however, the effectiveness distributions downstream of injection holes alter remarkably at the higher St_c. In the case of simple angle injection (Fig. 6(a)), the effectiveness values are largest at $M = 0.5$ and then decrease as M increases because of the injectant lift-off from the surface at the higher blowing ratios. With pulsations, the effectiveness values are significantly reduced compared to steady values. Another important fact is that the effectiveness values at $M = 1.0$ ($St_c = 1.8$) is now largest. The effectiveness values at $M = 0.5$ ($St_c = 3.6$) are smaller than those at $M = 1.0$, and are at the nearly same level with those at $M = 2.0$ ($St_c = 0.9$). This is because the pulsations play a most significant role at $M = 0.5$. This fact can also be expected from the phase-averaged static pressure difference shown in Fig. 2. The effectiveness is generally known to be higher at lower blowing ratios, but in real operating

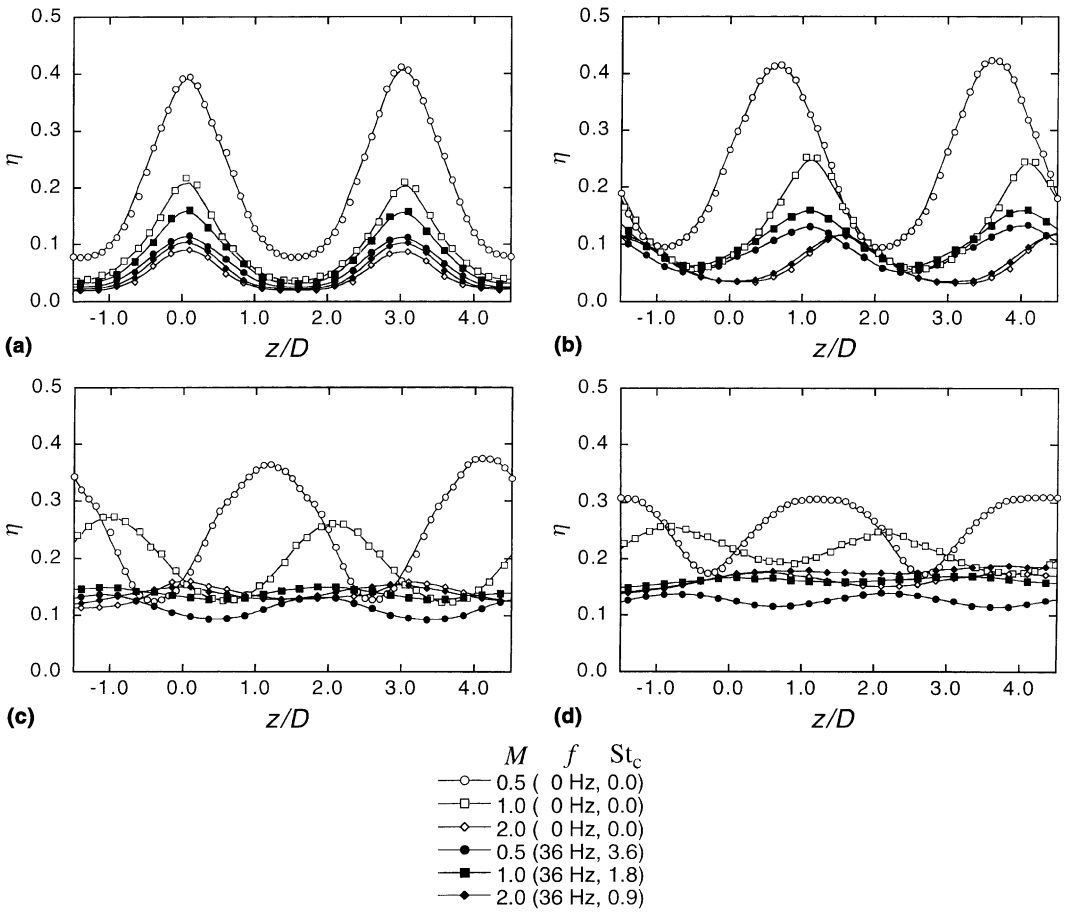

Fig. 6. Spanwise variation of the local adiabatic film cooling effectiveness at $x/D = 5.0$: (a) $\beta = 0°$; (b) $\beta = 30°$; (c) $\beta = 60°$; (d) $\beta = 90°$.

conditions it could be lower due to the unsteadiness at the high St_c.

The magnitude of reduction in the unsteady effectiveness values depends strongly on the Strouhal number and pressure parameter. The reduction is largest at $M = 0.5$ because St_c value (or pressure parameter) is largest in this case. For example, the peak value at $z/D = 0$ is reduced from the steady value 0.40 to the unsteady value 0.12. As the Strouhal number decreases (or the blowing ratio increases), the amount of reduction from the steady value also decreases. An interesting thing is that at $M = 2.0$, the unsteady values are even slightly larger than the steady values. At a higher blowing ratio such as $M = 2.0$, the steady effectiveness value is in general small because of the lift-off from the surface. However, this lift-off effect is now compensated by the pulsation effect that tends to keep the injectant trajectory closer to the surface.

With the 30° compound angle injection (Fig. 6(b)), the general trend of the effectiveness distributions are similar to those with simple angle injection except that the distributions are shifted and getting slightly more uniform in the spanwise direction. Here, again, the unsteady effectiveness values at $M = 0.5$ are smaller than those at $M = 1.0$, and are at the nearly same level with those at $M = 2.0$. In the steady case at $M = 0.5$, the location of the peak effectiveness is shifted by $z/D = 0.7$ in the z-direction. The shift is solely due to the spanwise momentum of the injectant. When pulsations are imposed, its location moves further in the z-direction to about $z/D = 1.15$. This is due to the spreading of the injectant caused by the unsteady oscillation. However, at $M = 1.0$ and 2.0, the peak locations of unsteady distributions are almost identical to those of steady ones because the spanwise momentum of the injectant is dominant over unsteady oscillation.

At 60° and 90° compound angle injections, the smoothing effect of pulsations is accelerated. The effectiveness in Figs. 6(c) and (d) shows more uniform distributions than that of small orientation angle. Other features such as the shift of peak value location and spreading in the z-direction are qualitatively the same as in the case of the 30° compound angle injection.

The space-averaged effectiveness, $\bar{\bar{\eta}}$, is compared in Fig. 7. The space-averaged effectiveness is determined by averaging the local effectiveness over the region of $-1.5 \leqslant z/D \leqslant 4.5$ and $1.0 \leqslant x/D \leqslant 16.0$. In general, the $\bar{\bar{\eta}}$ value increases with the orientation angle in both steady and unsteady cases. The amount of reduction in the averaged effectiveness value due to pulsations is greatest at $M = 0.5$. As the blowing ratio increases, the unsteady effectiveness value is approaching to be the same as the steady one at $M = 2.0$. The reduction in the space-averaged effectiveness value depends on the orientation angle as well as the blowing ratio. The amount of reduction due to pulsations decreases as the orientation angle increases at $M = 0.5$. For example, the space-averaged effectiveness value is reduced by 72% for simple angle injection and 45% for the 90° orientation angle injection. However, the amount of reduction increases with the orientation angle at $M = 1.0$.

It should also be noted that at the small orientation angles such as $\beta = 0°$ and 30°, the maximum occurs at $M = 1.0$ while at $\beta = 60°$ and 90°, the space-averaged effectiveness increases with the blowing ratio to a maximum value at $M = 2.0$. This is obviously because both the pulsation and orientation angle effects deteriorate more severely the film cooling performance at the smaller blowing ratios. It is generally accepted that the film protection is better at the smaller blowing ratios. However, considering the pulsation effect, it could

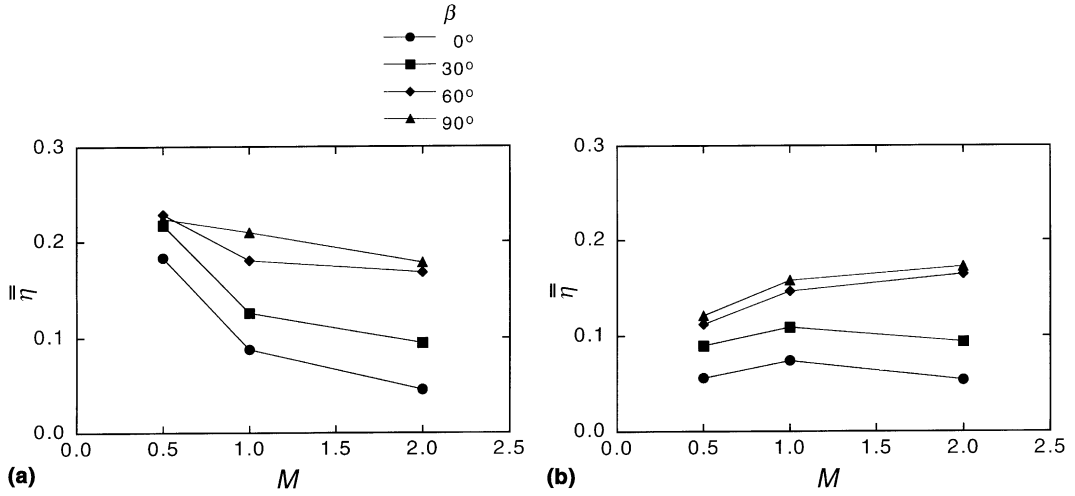

Fig. 7. Space-averaged adiabatic film cooling effectiveness: (a) $f = 0$ Hz (steady); (b) $f = 36$ Hz ($St_c = 3.60$).

be worse at the smaller blowing ratios. This observation is important because in a real engine, the turbine blades are operated with high frequency pulsations. Both the pulsation and the compound angle should be considered for the design of the turbine blade cooling system.

4. Conclusions

The effect of bulk flow pulsations on film cooling with a row of compound angle film cooling holes is investigated. The pulsations are in the form of near-sinusoidal velocity and static pressure wave forms at a frequency of 36 Hz. With this pulsation frequency, three different values of coolant Strouhal numbers of 0.9, 1.8 and 3.6 are produced according to the blowing ratios of 2.0, 1.0 and 0.5, respectively. The orientation angles considered are 0°, 30°, 60° and 90° at a fixed inclination angle of 35°. The phase-averaged and the time-averaged boundary layer temperature distributions are measured in the spanwise/normal planes downstream of the injection holes. The adiabatic film cooling effectiveness distributions are measured in detail with TLC. Some important observations are noted and summarized below.

1. Due to the pulsations, the free-stream static pressure could be higher than the plenum pressure at certain instants in a pulsation period. This might cause flow ingestion into the injection hole, especially at the high Strouhal numbers.
2. When the coolant Strouhal number is greater than unity, the phase-averaged boundary layer temperature distributions show important changes in the instantaneous injectant mass flow rate.
3. The time-averaged boundary layer temperature surveys show that pulsations induce large disruptions to the boundary layer temperature distribution and the film coverage. Diffusion is increased and the injectant spreads further over the wall with imposed pulsations.
4. Detailed investigation of the adiabatic film cooling effectiveness distributions reveals that a higher and more uniform effectiveness can be achieved at blowing ratios ranging from 0.5 to 2.0 with the increase in the orientation angle.
5. With pulsations the adiabatic film cooling effectiveness value decreases regardless of the orientation angle. The amount of reduction, however, depends on the orientation angle in such a way that the larger the orientation angle, the smaller the reduction.
6. It is generally accepted that the film protection is better at the smaller blowing ratios. However, considering the pulsation effect, it could be worse at the smaller blowing ratios.

References

[1] P. Sathyamurthy, S.V. Patankar, Prediction of film cooling with lateral injection, Heat Transfer Turbulent Flows, ASME-HTD 138 (1990) 61–70.
[2] P.M. Ligrani, S. Ciriello, D.T. Bishop, Heat transfer, adiabatic effectiveness, and injectant distributions downstream of a single row and two staggered rows of compound angle film-cooling holes, ASME J. Turbomach. 114 (1992) 687–700.
[3] P.M. Ligrani, J.M. Wigle, S. Ciriello, S.M. Jackson, Film cooling from holes with compound angle orientations, Part1: Results downstream of two staggered rows of holes with 3d spanwise spacing, ASME J. Turbomach. 116 (1994) 341–352.
[4] B. Sen, D.L. Schmidt, D.G. Bogard, Film cooling with compound angle holes: Heat transfer, ASME Paper No. 94-GT-312, in: Proceedings of the 39th ASME International Gas Turbine and Aeroengine Congress and Exposition, 1994.
[5] D.L. Schmidt, B. Sen, D.G. Bogard, Film cooling with compound angle holes: Adiabatic effectiveness, ASME Paper No. 94-GT-312, in: Proceedings of the 39th ASME International Gas Turbine and Aeroengine Congress and Exposition, 1994.
[6] S. Honami, T. Shizawa, A. Uchiyama, Behavior of the laterally injected jet in film cooling: measurements of surface temperature and velocity/temperature field within the jet, ASME J. Turbomach. 116 (1994) 106–112.
[7] P.M. Ligrani, J.S. Lee, Film cooling from a single row of compound angle holes at high blowing ratios, Int. J. Rotating Mach. 2 (1996) 259–267.
[8] S.V. Ekkad, D. Zapata, J.-C. Han, Film effectiveness over a flat surface with air and injection through compound angle holes using a transient liquid crystal image method, ASME J. Turbomach. 119 (1997) 587–593.
[9] P.M. Ligrani, A.E. Ramsey, Film cooling from spanwise oriented holes in two staggered rows, ASME J. Turbomach. 119 (1997) 562–567.
[10] S.W. Lee, Y.B. Kim, J.S. Lee, Flow characteristics and aerodynamic losses of film-cooling jets with compound angle orientations, ASME J. Turbomach. 119 (1997) 310–319.
[11] M.G. Dunn, W.A. Bennett, R.A. Delaney, K.V. Rao, Investigation of unsteady flow through a transonic turbine stage: Data/prediction comparison for time-averaged and phase-resolved pressure data, ASME J. Turbomach. 114 (1992) 91–99.
[12] K.V. Rao, R.A. Delaney, M.G. Dunn, Vane–blade interaction in a transonic turbine, part I: aerodynamics, J. Propulsion Power 10 (3) (1994) 305–311.
[13] R.S. Abhari, A.H. Epstein, An experimental study of film cooling in a rotating transonic turbine, ASME J. Turbomach. 116 (1994) 63–70.
[14] R.S. Abhari, Impact of rotor–stator interaction on turbine blade film cooling, ASME J. Turbomach. 118 (1996) 103–113.
[15] P.M. Ligrani, R. Gong, J.M. Cuthrell, J.S. Lee, Bulk flow pulsations and film cooling – I. Injectant behavior, Int. J. Heat Mass Transfer 39 (1996) 2271–2282.

[16] P.M. Ligrani, R. Gong, J.M. Cuthrell, J.S. Lee, Bulk flow pulsations and film cooling – II. Flow structure and film effectiveness, Int. J. Heat Mass Transfer 39 (1996) 2283–2292.

[17] P.M. Ligrani, R. Gong, J.M. Cuthrell, J.S. Lee, Effects of bulk flow pulsations on film-cooled boundary layer structure, ASME J. Fluids Eng. 119 (1997) 56–66.

[18] D.K. Sohn, J.S. Lee, The effect of bulk flow pulsations on film cooling from two rows of holes, ASME Paper No. 97-GT-129, in: Proceedings of the 42nd ASME International Gas Turbine and Aeroengine Congress and Exposition, 1997.

[19] S.J. Kline, F.A. McClintock, Describing uncertainties in single sample experiments, Mech. Eng. 75 (1953) 3–8.